

The dynamics of Galactic centre pulsars: constraining pulsar distances and intrinsic spin-down

B. B. P. Perera,^{1*} E. D. Barr,² M. B. Mickaliger,¹ A. G. Lyne,¹ D. R. Lorimer,^{3,4}
 B. W. Stappers,¹ R. P. Eatough,² M. Kramer,^{2,1} C. Ng,⁵ R. Spiewak,⁶ M. Bailes,^{6,7}
 D. J. Champion,² V. Morello¹ and A. Possenti⁸

¹ *Jodrell Bank Centre for Astrophysics, School of Physics and Astronomy, The University of Manchester, Manchester M13 9PL, UK*

² *Max-Planck-Institut für Radioastronomie, Auf dem Hügel 69, D-53121 Bonn, Germany*

³ *Department of Physics and Astronomy, West Virginia University, Morgantown, WV 26506, USA*

⁴ *Center for Gravitational Waves and Cosmology, West Virginia University, Chestnut Ridge Research Building, Morgantown, WV 26505, USA*

⁵ *Department of Physics and Astronomy, University of British Columbia, 6224 Agricultural Road, Vancouver, BC V6T 1Z1, Canada*

⁶ *Centre for Astrophysics and Supercomputing, Swinburne University of Technology, PO Box 218, Hawthorn, VIC 3122, Australia*

⁷ *ARC Centre of Excellence for Gravitational Wave Discovery (OzGrav), Swinburne University of Technology, PO Box 218, VIC 3122, Australia*

⁸ *INAF - Osservatorio Astronomico di Cagliari, via della Scienza 5, I-09047 Selargius (CA), Italy*

ABSTRACT

Through high-precision radio timing observations, we show that five recycled pulsars in the direction of the Galactic Centre (GC) have anomalous spin period time derivative (\dot{P}) measurements – PSRs J1748–3009, J1753–2819, J1757–2745, and J1804–2858 show negative values of \dot{P} and PSR J1801–3210 is found to have an exceptionally small value of \dot{P} . We attribute these observed \dot{P} measurements to acceleration of these pulsars along their lines-of-sight (LOSs) due to the Galactic gravitational field. Using models of the Galactic mass distribution and pulsar velocities, we constrain the distances to these pulsars, placing them on the far-side of the Galaxy, providing the first accurate distance measurements to pulsars located in this region and allowing us to consider the electron density along these LOSs. We find the new electron density model YMW16 to be more consistent with these observations than the previous model NE2001. The LOS dynamics further constrain the model-dependent intrinsic \dot{P} values for these pulsars and they are consistent with measurements for other known pulsars. In the future, the independent distance measurements to these and other pulsars near the GC would allow us to constrain the Galactic gravitational potential more accurately.

Key words: stars: neutron – pulsars: general – pulsars: individual: PSR J1753–2819, J1746–2758, J1748–3009, J1757–2745, J1801–3210, J1804–2858 – stars: distances – stars: kinematics and dynamics – galaxies: kinematics and dynamics

1 INTRODUCTION

Pulsars are among the most reliable macroscopic periodic sources in the universe and their long-term stability is comparable to that of atomic clocks (e.g. Petit & Tavella 1996; Hobbs et al. 2012). This allows the parameters of pulsars to be measured to exquisite precision through measuring and modelling the arrival times of their pulses (e.g. Kaspi et al. 1994). These measurements are sensitive to any dynamical

changes caused by external forces on the pulsar such as the gravitational forces exerted by other masses (e.g. Freire et al. 2017; Perera et al. 2017).

Pulsars are thought to be powered by the loss of rotational kinetic energy and thus, gradually spin down over time, leading to positive values of \dot{P} . The current pulsar population strongly supports this hypothesis with measured positive \dot{P} values for the vast majority of pulsars¹ (see

* E-mail: bhakthiperera@gmail.com

¹ <http://www.atnf.csiro.au/people/pulsar/psrcat>

Manchester et al. 2005). However, some pulsars, located in globular clusters, show significant negative \dot{P} measurements (e.g. Wolszczan et al. 1989; Freire et al. 2017; Jacoby et al. 2006; Corongiu et al. 2006; Lynch et al. 2012). These \dot{P} values are not entirely intrinsic, but induced by the dynamics due to the LOS component of the acceleration of the pulsar, mainly in the gravitational potential of the cluster itself, locating them on the far-side of the cluster (see, e.g., Freire et al. 2003, 2017).

Similar to the globular clusters, the Galaxy has a strong gravitational potential within the central regions due to the high stellar and gas densities. We therefore expect negative \dot{P} measurements from pulsars that are located near the Galactic centre (GC) on the far-side of the Galaxy (see § 5.1 for details). However, prior to this work, there was no conclusive evidence for this. As we show below using our timing observations, PSRs J1748–3009 (Knispel et al. 2013), J1753–2819 (originally announced by Mickaliger 2013), J1757–2745 (Ng et al. 2015), and J1804–2858 (Morello et al. 2019, Barr et al., *in prep*) all show significant negative \dot{P} measurements, and PSR J1801–3210 (Ng et al. 2014) shows a remarkably small but positive \dot{P} measurement when compared to the known pulsar population.

In addition to the pulsars listed above, we note that our timing of PSR J1746–2758 (Ng et al. 2015) does not show an unusual \dot{P} measurement, however, its location in the Galaxy and some measured properties have similarities to those of above mentioned pulsars, making it useful to consider in this work. The previously reported rotational, and some other measured and derived parameters, for these pulsars are given in Table 1, noting that four of them had no previous \dot{P} measurements. All six pulsars considered here are located along LOSs which pass near the GC with an angular separation of $< 5^\circ$. With their comparably large dispersion measure (DM – which accounts for the frequency-dependent time delay of the radio pulses due to electrons in the inter-stellar medium along the LOS) values, it is likely that these pulsars are located within the inner regions of the Galaxy around the GC (Cordes & Lazio 2002; Yao et al. 2017). Given the special locations of these pulsars, it is likely that their unusual observed \dot{P} measurements are not entirely intrinsic, but rather induced by the pulsar acceleration in the Galactic gravitational potential. We further note that these pulsars are useful in studying the DM environment of the inner region of the Galaxy.

The paper is organized as follows. In § 2, we describe the discovery observations of PSR J1753–2819. In § 3, we present our observations and data processing of all six pulsars. We then discuss the timing analysis of these pulsars in § 4 and report their negative/small observed \dot{P} measurements. We analyse their dynamics in § 5, including the LOS accelerations combining the Galactic mass distribution and pulsar velocity models (§ 5.1 and 5.2), leading to limits on their intrinsic \dot{P} values (§ 5.3) and their possible distances (§ 5.4). We compare our dynamically-derived distances with DM-derived distances obtained using electron density models in § 5.5. Finally in § 6, we discuss our results and present conclusions.

2 DISCOVERY OF PSR J1753–2819

The Parkes Multibeam Pulsar Survey (PMPS – Manchester et al. 2001) has significantly expanded the known pulsar population, resulting in over 800 new pulsar discoveries to-date (Morris et al. 2002; Kramer et al. 2003; Hobbs et al. 2004a; Faulkner et al. 2004; Lorimer et al. 2006; Eatough et al. 2009, 2010, 2013; Keith et al. 2009; Mickaliger et al. 2012; Knispel et al. 2013), including 21 millisecond pulsars and 30 rotating radio transients. The PMPS was carried out as a blind pulsar survey along the Galactic plane with $|b| < 5^\circ$ using the 13-beam multibeam receiver (with a centre frequency of 1374 MHz and a bandwidth of 288 MHz) on the Parkes radio telescope (PKS) in Australia. Due to advanced and improved pulsar search pipelines being applied to the archival PMPS data, and independent visual inspection of the candidate output plots, five new millisecond pulsars were discovered and reported by Mickaliger et al. (2012).

These methods also resulted in the discovery of PSR J1753–2819 (originally announced by Mickaliger 2013). As described by Mickaliger et al. (2012), the PMPS data were initially dedispersed using `dedisperse_all`², a multi-threaded dedisperser compatible with the SIGPROC software package (Lorimer 2011). The resulting time series were then searched using `seek`³. For statistically significant candidates, the raw data were folded at the candidate period using `prepfold` from the PRESTO software package⁴ (Ransom 2011). The number of candidates was reduced by selecting those within a parameter space from which pulsars were likely to have been previously missed, i.e. spin period $P < 50$ ms, $DM > 10$ pc cm⁻³. The resulting folded candidates were viewed by eye and confirmation observations were performed and were reported by Mickaliger et al. (2012). This search was undertaken as part of a larger search for fast radio bursts, which classified single pulses from known pulsars detected in the PMPS (Mickaliger et al. 2018). Like the five pulsars reported in Mickaliger et al. (2012), PSR J1753–2819 was probably missed in earlier searches of the PMPS due to its high DM, short spin period, and binary nature, as well as the large number of candidates present in those searches. Further details of the search are reported in Mickaliger et al. (2012).

3 OBSERVATIONS AND DATA PROCESSING

We observed PSRs J1748–3009, J1746–2758, J1757–2745, J1801–3210, and J1804–2858 using the Lovell Telescope (LT) at the Jodrell Bank Observatory in the UK approximately monthly or semi-monthly since their discoveries. After confirming the discovery of PSR J1753–2819, it was observed using the LT approximately every 17 days. All these observations were carried out at ‘L band’ at a centre frequency of 1532 MHz and a bandwidth of 400 MHz. The data were recorded using the ‘ROACH’ pulsar backend (Bassa et al. 2016a). The observation details are given in Table 2. In addition to the ROACH data sets, PSR J1801–3210

² <https://github.com/swinlegion/sigproc>

³ <http://sigproc.sourceforge.net>

⁴ <https://www.cv.nrao.edu/~sransom/presto>

Table 1. The previously published parameters of the pulsars in this study. The distance is estimated using the electron density models given in Yao et al. (2017)(YMW16) and Cordes & Lazio (2002)(NE2001). Since there are no multi-frequency observations in this study, we use these published DM measurements and keep them fixed in our timing models.

PSR	l ($^{\circ}$)	b ($^{\circ}$)	P (ms)	\dot{P} (s/s)	DM (cm^{-3} pc)	Ref.	$D_{\text{YMW16}}^{\dagger\dagger}$ (kpc)	$D_{\text{NE2001}}^{\dagger\dagger}$ (kpc)
J1746–2758 [†]	0.97	0.49	487.53	–	422.0	1	4.2	5.2
J1748–3009	359.27	–1.15	9.68	–	420.2	2	5.1	5.1
J1753–2819	1.46	–1.25	18.62	–	298.0	3	4.1	4.5
J1757–2745 [†]	2.40	–1.72	17.69	$2.1(2) \times 10^{-19}$	334.0	1	5.2	5.2
J1801–3210	358.92	–4.58	7.45	$-4(4) \times 10^{-23}$	177.7	4, 5	6.1	4.0
J1804–2858	1.99	–3.50	1.49	–	232.4	6, 7	8.2	4.9

[†]PSRs J1746–2758 and J1757–2745 were previously published as J1746–27 and J1757–27, respectively, due to lack of precision in their positions.

^{††}Note that YMW16 and NE2001 used the distance of the Sun from the GC as 8.3 kpc and 8.5 kpc, respectively. However, the systematic offset introduced by this difference in the distance measurement is much smaller than the uncertainty of these electron density models.

References: (1) Ng et al. (2015); (2) Knispel et al. (2013); (3) Mickaliger (2013); (4) Bates et al. (2011); (5) Ng et al. (2014); (6) Morello et al. (2019); (7) Barr et al. (in preparation)

was observed using the LT with the ‘DFB’ backend between February 2010 and April 2011. The ‘DFB’ observations were carried out at a slightly different centre frequency of 1520 MHz and a bandwidth of 384 MHz. We used both data sets of this pulsar in the analysis to extend its time baseline.

In addition to the LT observations, PSRs J1801–3210 and J1804–2858 were observed using the Parkes radio telescope since their discoveries. These observations were also taken at ‘L band’ with a centre frequency of 1369 MHz and a bandwidth of 400 MHz and recorded with the CASPSR backend (see Table 2). We noticed that some of the calibration observations obtained from PKS as a part of PMPS in the period between December 1998 and August 2001 happened to overlap with the position of PSR J1748–3009, that is, prior to its discovery. Therefore, we used these data and folded them using the pulsar ephemeris and included the resultant detections in our timing analysis. These observations were carried out at 1374 MHz with a bandwidth of 288 MHz and recorded using the ‘analogue filter bank’ (AFB) backend. When combined with the existing data set this extended the observation baseline of PSR J1748–3009 by more than 13 years, we were able to significantly improve the timing measurements while fitting for new timing model parameters (see § 4).

We processed these data using the pulsar analysis software package PSRCHIVE⁵(Hotan et al. 2004; van Straten et al. 2012, 2011). We folded each observation for its entire length and summed all the frequency channels together to form the integrated pulse profile. A time-of-arrival (TOA) was generated by cross-correlating each of the integrated pulse profiles with a noise-free profile template (Taylor 1992) using *pat*⁶ in PSRCHIVE. This resulted in 83, 169, 98, 75, 187, and 101 TOAs for

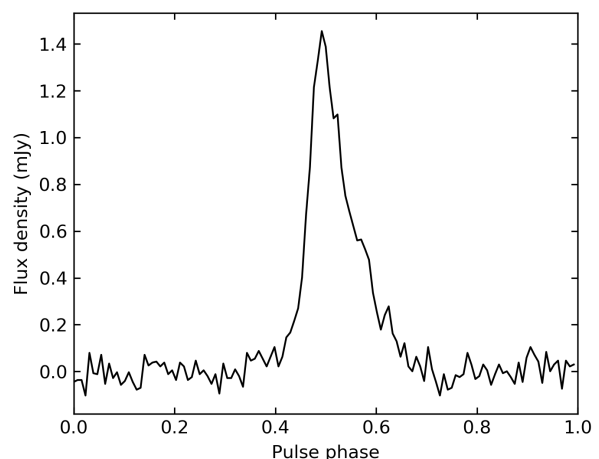


Figure 1. Integrated pulse profile of recently discovered PSR J1753–2819. Note that the y-axis is scaled in flux density. The mean flux density is estimated to be 0.14 mJy and the pulse widths at 50% and 10% of the peak are estimated to be $W_{50} = 1.51$ ms and $W_{10} = 3.98$ ms, respectively.

PSRs J1746–2758, J1748–3009, J1753–2819, J1757–2745, J1801–3210, and J1804–2858, respectively.

Fig. 1 shows the integrated pulse profile of PSR J1753–2819 as it was not published in the original announcement (Mickaliger 2013). We estimate the flux density of the pulsar using the radiometer equation (see Lorimer & Kramer 2005), with the system temperature of $T_{\text{sys}} = 42$ K (i.e. $T_{\text{sky}} = 12$ K in the direction of the pulsar according to Haslam et al. (1982) with a spectral index of -2.6 and $T_{\text{rec}} + T_{\text{spill}} = 30$ K) and the telescope gain of 0.9 K/Jy, and scale the profile accordingly. These calculations estimate the mean flux density of the pulsar to be 0.14 mJy. We further measure the pulse width, at 50% and 10% of the peak to be $W_{50} = 1.51$ ms and $W_{10} = 3.98$ ms, respectively.

⁵ <http://psrchive.sourceforge.net>

⁶ we used the FDM (Fourier domain with Markov chain Monte Carlo) method.

Table 2. The observation details of pulsars in this analysis. From left to right, we list the pulsar name, telescope used, centre observing frequency and bandwidth, number of bins in the integrated pulse profile and number of observations.

PSR	Telescope Backend	Centre Freq (MHz)	Bandwidth (MHz)	Phase bins	Data span	No. of observations
J1746–2758	LT/ROACH	1532	400	1024	12/2013 – 4/2018	82
J1748–3009	LT/ROACH	1532	400	1024	5/2012 – 11/2018	146
	PKS/AFB	1374	288	32	12/1998 – 8/2001	23
J1753–2819	LT/ROACH	1532	400	1024	9/2012 – 10/2018	94
J1757–27	LT/ROACH	1532	400	1024	3/2014 – 10/2018	80
J1801–3210	LT/ROACH	1532	400	1024	4/2011 – 10/2018	74
	LT/DFB	1520	384	1024	7/2009 – 4/2011	60
	PKS/CASPSR	1369	400	256	7/2010 – 4/2018	53
J1804–2858	LT/ROACH	1532	400	256	12/2013 – 3/2018	46
	PKS/CASPSR	1369	400	256	12/2013 – 4/2018	55

4 TIMING PULSARS

We fit timing models including astrometric and rotational frequency parameters for PSRs J1746–2758, J1748–3009, J1753–2819, J1757–2745, J1801–3210, and J1804–2858 to the TOAs. The timing solutions are improved by minimising the χ^2 value of the timing residuals between the observed and model-predicted TOAs using the pulsar timing software TEMPO2 (Edwards et al. 2006; Hobbs et al. 2006; Hobbs & Edwards 2012). Since we do not have multi-frequency observations, we keep the DM of the pulsar fixed at its previously published value (see Table 1). Note that PSRs J1748–3009, J1753–2819, and J1801–3210 are in binary orbits and thus, we include Keplerian parameters in their timing models (see Lorimer & Kramer 2005) using the binary model ‘BT’ (Blandford & Teukolsky 1976). When TOAs from different telescopes/backends are available (see Table 2), we combined them by fitting for a time offset (‘JUMP’) in the timing model of the pulsar to take into account any systematic delays between the data sets. During the fitting process, the topocentric TOAs are converted to the Solar-system barycentric coordinate time (TCB) using the DE436⁷ ephemeris (Folkner et al. 2009) and placed on the Terrestrial Time standard BIPM2015⁸. The resultant timing parameters of our pulsars are given in Table 3 and 4.

4.1 PSR J1748–3009

This binary millisecond pulsar has a spin period of 9.7 ms and is located with an angular separation of $1^\circ 36'$ from the GC (see Table 5). Based on about 20 years of our timing data, by combining the early PKS observations with LT observations, the timing parameters of the pulsar improved significantly. The timing model constrains the \dot{P} measurement of the pulsar for the first time to be $-3.580(2) \times 10^{-20}$ s/s. This negative value indicates that the measured \dot{P} is not entirely intrinsic, rather induced by the acceleration of the pulsar due to the Galactic potential, and we constrain the limit on the intrinsic value based on dynamics in § 5.3. We

⁷ This new solar-system ephemeris DE436 is based on Folkner et al. (2014).

⁸ This time standard has been obtained according to principles given in Guinot (1988) and Petit (2003).

further find that the timing solution of the pulsar requires a second time derivative of the rotational frequency (\ddot{f}), with an approximately 7σ significance (see Table 3), to achieve white residuals. Our timing analysis also places a limit on the orbital period time derivative \dot{P}_b of the pulsar with a significance of 2.6σ . We use this limit independently to further constrain the intrinsic period derivative of the pulsar in § 5.3.

4.2 PSR J1753–2819

The newly discovered PSR J1753–2819 (Mickaliger 2013) is a 18.6 ms mildly-recycled pulsar in a 9.3-hr binary orbit (see Table 3) with a DM of $298 \text{ cm}^{-3} \text{ pc}$. It is located at an angular separation of $1^\circ 92'$ from the GC, resulting in a projected separation of 275 pc in the sky-plane at the distance of the GC (see Table 5). Initial timing observations during the discovery showed a mild evidence for a negative \dot{P} , and the current value is measured to be $-4.94(2) \times 10^{-20}$ s/s based on our 6 years of LT observations. This negative \dot{P} value indicates that this measurement is also affected by the pulsar dynamics in the Galactic potential (see § 5.3).

4.3 PSR J1757–2745

PSR J1757–2745 is an isolated mildly-recycled pulsar with a spin period of 17.7 ms and located at an angular separation of $2^\circ 95'$ from the GC (see Table 5). Our 4.5 years of observations improved its timing solution, updating the \dot{P} measurement to be $-1.30(2) \times 10^{-20}$ s/s (see Table 4). This negative value indicates that this \dot{P} measurement is also affected by the pulsar dynamics in the Galactic potential, and we study this in detail (see § 5.3). The timing analysis also places a limit on the proper motion, particularly in Right Ascension (see Table 4).

The previous timing analysis of this pulsar reported a \dot{P} measurement of $2.1(2) \times 10^{-19}$ s/s (Ng et al. 2015) based on a short time span of 206 days. However, we now confirm that this value is not correct due to the short data span and resultant large covariance between the rotational and astrometric parameters.

Table 3. The timing model parameters of the newly discovered PSR J1753–2819 and the updated timing model parameters of PSRs J1746–2758, and J1748–3009. Due to the lack of multi-frequency observations, we present the DM values (and their uncertainties, if available) reported in their discovery analyses and kept them fixed. The 1σ uncertainties of measurements are given in parentheses. The characteristic age ($\tau = P/2\dot{P}$) and the surface magnetic field ($B_S = 3.2 \times 10^{19} \sqrt{P\dot{P}}$ G) are computed based on the intrinsic \dot{P} limits estimated using the dynamics of each pulsar as described in § 5.3.

Timing parameter	J1746–2758	J1748–3009	J1753–2819
Data span (MJD)	56639 – 58423	51148 – 58428	56174 – 58423
Number of TOAs	82	169	94
Weighted rms timing residual (μs)	545	86	82
Reduced χ^2 value	1.00	0.99	0.99
Units	TCB	TCB	TCB
Measured parameters:			
Right ascension RA (J2000)	17:45:52.248(3)	17:48:23.7582(3)	17:53:56.1837(4)
Declination Dec. (J2000)	–27:58:38.0(5)	–30:09:11.28(4)	–28:19:30.03(7)
Spin frequency f (s^{-1})	2.051164249099(9)	103.26352668931(4)	53.69521954620(1)
Spin frequency 1 st derivative \dot{f} (s^{-2})	$-1.86(2) \times 10^{-17}$	$3.817(2) \times 10^{-16}$	$1.423(4) \times 10^{-16}$
Spin frequency 2 nd derivative \ddot{f} (s^{-3})	$-4.9(19) \times 10^{-26}$	$-2.2(3) \times 10^{-26}$	–
Reference epoch (MJD)	57531	54788	57299
Dispersion measure DM (cm^{-3} pc)	422(9)	420.2	298
Orbital period P_b (d)	–	2.93382034(2)	0.387677373(3)
Epoch of periastron T_o (MJD)	–	56999.183308(4)	56999.821829(4)
Projected semi-major axis x (lt-s)	–	1.320085(9)	0.20967(1)
Orbital period derivative \dot{P}_b (s/s)	–	$-2.6(10) \times 10^{-11}$	–
Derived parameters:			
Gal. longitude l (deg)	0.8473(1)	359.272301(8)	1.46179(2)
Gal. latitude b (deg)	0.45243(8)	–1.147126(6)	–1.25174(1)
Spin period P (s)	0.487527998033(2)	0.009683961337179(4)	0.018623631832617(5)
Spin period derivative \dot{P} (s/s)	$4.42(5) \times 10^{-18}$	$-3.580(2) \times 10^{-20}$	$-4.94(2) \times 10^{-20}$
Intrinsic \dot{P} (s/s)	$<1.48 \times 10^{-17}$	$<1.38 \times 10^{-19}$	$<2.08 \times 10^{-19}$
Characteristic age τ (Gyr)	>0.5	>1.1	>1.4
Surface magnetic field B_S ($\times 10^9$ G)	<85	<1.1	<2.0
Companion mass (M_\odot)	–	0.08 – 0.20	0.05 – 0.12

4.4 PSR J1801–3210

PSR J1801–3210 has a spin period of 7.45 ms and is located at an angular separation of 4.7° from the GC (see Table 5). As shown in Table 4 based on our 9 yr data set, we find improved timing parameters of the pulsar, indicating that \dot{P} measurement is constrained to be a positive value of $7.4(8) \times 10^{-23}$ s/s. This measurement is still smaller than the lowest positive \dot{P} measured to-date for any known pulsar⁹.

The previous timing analysis of this pulsar showed a low-significance \dot{P} measurement of $-4(4) \times 10^{-23}$ s/s based on a 4 yr long data set (Ng et al. 2014). They argued that the pulsar is possibly located behind the sky-plane which passes through the GC along the LOS. In that case the negative Galactic acceleration affects the positive intrinsic spin-down of the pulsar and results in an extremely low measured \dot{P} value (see § 5.1 for details). Although the DM-derived distance from the NE2001 electron density model places the pulsar in front of the sky-plane (see Table 1), they argued that the electron density models can contain large uncertainties. Therefore, our exceptionally small \dot{P} measurement indicates the scenario of the pulsar being located behind the sky-plane through the GC proposed by Ng et al. (2014) is still valid (which we will show independently in § 5.4).

⁹ <http://www.atnf.csiro.au/people/pulsar/psrcat>

4.5 PSR J1804–2858

PSR J1804–2858 is a solitary millisecond pulsar and has the third lowest spin period known to-date, a spin period of 1.49 ms (Morello et al. 2019, Barr et al., *in prep*). It is located at an angular radius of 4° from the GC (Table 5) and the DM is 232 cm^{-3} pc, which places the pulsar at a distance of 8.2 kpc from the Earth based on the YMW16 electron density model (see Table 1). The discovery analysis of the pulsar did not have a \dot{P} measurement, however our 4.3 years of timing data measures a significant \dot{P} value of $-7.57(2) \times 10^{-22}$ s/s (see Table 4). As mentioned above for other pulsars, this measured \dot{P} value is not entirely intrinsic, rather induced by the acceleration of the pulsar along its LOS due to the Galactic potential. We study its dynamics in detail combining with the Galactic mass distribution and constrain the intrinsic \dot{P} value in § 5.3.

4.6 PSR J1746–2758

This isolated 0.49-s spin period pulsar has an angular separation of just $0^\circ.96$ from the GC (see Table 5). Our updated timing solution based on more than four years of observations indicates a \dot{P} measurement for the first time to be $4.42(5) \times 10^{-18}$ s/s (see Table 3). Comparing this measurement with \dot{P} values of known pulsars that have a similar

Table 4. Same as Table 3, but for PSRs J1757–2745, J1801–3210, and J1804–2858.

Timing parameter	J1757–2745	J1801–3210	J1804–2858
Data span (MJD)	56728 – 58422	55032 – 58423	56638 – 58213
Number of TOAs	80	187	101
Weighted rms timing residual (μ s)	12	28	8
Reduced χ^2 value	0.98	0.99	0.97
Units	TCB	TCB	TCB
Measured parameters:			
Right ascension RA (J2000)	17:57:54.7826(1)	18:01:25.8872(1)	18:04:01.52323(4)
Declination Dec. (J2000)	–27:45:40.16(2)	–32:10:53.733(9)	–28:58:46.608(7)
Proper motion in RA, PMRA (mas/yr)	–11.4(11)	–4.0(6)	–6.4(5)
Proper motion in Dec., PMDEC (mas/yr)	54(17)	–4(3)	–11(5)
Spin frequency f (s^{-1})	56.538013330516(8)	134.16363857905(1)	669.93358254482(5)
Spin frequency 1 st derivative \dot{f} (s^{-2})	$4.17(5) \times 10^{-17}$	$-1.3(2) \times 10^{-18}$	$3.399(9) \times 10^{-16}$
Spin frequency 2 nd derivative \ddot{f} (s^{-3})	$-4.7(18) \times 10^{-26}$	$-2.5(5) \times 10^{-26}$	$-2.6(9) \times 10^{-25}$
Spin frequency 3 rd derivative \dddot{f} (s^{-4})	$-5.1(14) \times 10^{-33}$	–	–
Reference epoch (MJD)	57575	56635	57425
Dispersion measure DM (cm^{-3} pc)	334	177.713(4)	232.4
Orbital period P_b (d)	–	20.77169953(3)	–
Epoch of periastron T_0 (MJD)	–	56518.268546(1)	–
Projected semi-major axis x (lt-s)	–	7.809320(3)	–
Derived parameters:			
Gal. longitude l (deg)	2.390743(5)	358.921963(2)	1.995292(2)
Gal. latitude b (deg)	–1.726491(3)	–4.577230(2)	–3.497440(1)
Spin period P (s)	0.017687215045108(3)	0.0074535843734652(5)	0.0014926852841164(1)
Spin period derivative \dot{P} (s/s)	$-1.30(2) \times 10^{-20}$	$7.4(8) \times 10^{-23}$	$-7.57(2) \times 10^{-22}$
Intrinsic \dot{P} (s/s)	$<1.42 \times 10^{-19}$	$<3.50 \times 10^{-20}$	$<7.92 \times 10^{-21}$
Characteristic age τ (Gyr)	>2.0	>3.4	>3.0
Surface magnetic field B_s ($\times 10^9$ G)	<1.6	<0.5	<0.1
Companion mass (M_\odot)	–	0.14 – 0.35	–

Table 5. Summary of the parameters of pulsars used in our dynamic analysis. The angular separation θ of the pulsar from the GC is calculated based on the Galactocentric coordinates (l, b) . The uncertainties of l , b , and θ are estimated based on the uncertainties of pulsar positions measured from timing (Table 3 and 4). The projected separation r_\perp of the pulsar from the GC in the sky plane is calculated based on a GC distance of 8.2 ± 0.1 kpc from the Sun (Bland-Hawthorn et al. 2019). Note that the uncertainty in r_\perp is dominated by the uncertainty in the GC distance.

PSR	l ($^\circ$)	b ($^\circ$)	θ ($^\circ$)	r_\perp (pc)	\dot{P}_{obs}/P ($\times 10^{-10}$ yr $^{-1}$)
J1746–2758	0.8473(1)	0.45243(8)	0.9605(1)	137(2)	2.86(3)
J1748–3009	359.272301(8)	–1.147126(6)	1.358445(7)	194(2)	–1.1657(6)
J1753–2819	1.46176(2)	–1.25174(1)	1.92438(1)	275(3)	–0.836(3)
J1757–2745	2.390743(5)	–1.726491(3)	2.94868(5)	422(5)	–0.233(3)
J1801–3210	358.921963(2)	–4.577230(2)	4.702204(2)	672(7)	0.0031(4)
J1804–2858	1.995292(2)	–3.497440(1)	4.025958(1)	576(6)	–0.1600(4)

pulse period, it is evident that this value is slightly smaller than the majority, but within the distribution. On the other hand, one can imagine, given the pulsar’s location, that it is closer to the GC than the DM-derived distance (see Table 1) and thus, the measured \dot{P} is not entirely intrinsic, but rather induced by the Galactic potential. However, such a claim is not likely to be straightforward. Further note that the maximum Galactic acceleration in the direction of the pulsar is greater than the measured \dot{P}/P and thus, we study its dynamics due to the Galactic potential in § 5.3 in detail.

5 DYNAMICS OF PULSARS

The timing models for PSRs J1748–3009, J1753–2819, J1757–2745, and J1804–2858 show negative observed \dot{P} measurements (see § 4), indicating that these values are not entirely intrinsic and have a dynamic contribution. We also note that the observed \dot{P} of PSR J1801–3210 is extremely small, so that it is also likely to be affected by dynamics (see § 4.4). In this section, we model the observed unusual \dot{P} measurements as being due to acceleration of these pulsars along their LOSs, and then constrain their intrinsic \dot{P} values and possible distances.

of the Galaxy (see Table 6 in Sofue 2017, for updated values). This study used observations covering the inner region (from ~ 1 pc) of the Galaxy and thus, required several bulge components to appropriately model the data.

For comparison, we also use the Galactic mass distribution model proposed by McMillan (2017). This model uses a main bulge, two stellar discs, two gas discs, and a dark halo. The McMillan (2017) model is an improved version of their previous model (McMillan 2011) which now includes gas discs and uses new observations of maser sources in the Galaxy. We note that these models mainly focus on the region beyond the bulge (where $r_{\perp} > 1$ kpc) in the Galaxy. Since our pulsars are likely located around the central region of the Galaxy (within a $r_{\perp} < 1$ kpc, see Table 5), we use the Sofue (2013) model with updated parameters given in Sofue (2017) as our main Galactic mass distribution model in the analysis.

Throughout the analysis, we assume the Galactocentric distance of the solar system to be $R_{\odot} = 8.2 \pm 0.1$ kpc and the central black hole mass to be $(4.2 \pm 0.2) \times 10^6 M_{\odot}$ (Bland-Hawthorn et al. 2019; Vasiliev 2019; Bland-Hawthorn & Gerhard 2016; Sofue 2013, 2017; McMillan 2017). These values are consistent with those derived in previous studies within their uncertainties (e.g. Genzel et al. 2000; Ghez et al. 2005, 2008; Gillessen et al. 2009; Reid et al. 2009; Honma et al. 2012; Schönrich 2012; Brunthaler et al. 2011; Reid et al. 2014). We further note that this R_{\odot} is broadly consistent with the recently measured GC distance, which has an uncertainty of only 0.3% (Abuter et al. 2019).

To be consistent with the above Galactic models (Sofue 2013; McMillan 2017), we define the volume mass density of the bulge component in cylindrical Galactocentric coordinates

$$\rho_b(R, z) = \frac{\rho_{0,b}}{(1 + r/r_0)^{\alpha}} \exp[-(r/r_{\text{cut}})^{\zeta}], \quad (2)$$

where, $\rho_{0,b}$ is the central mass density and $r = \sqrt{R^2 + (z/q)^2}$ with the axis ratio q . Sofue (2013) includes two bulges with $\zeta = 1$, $\alpha = 0$, $r_0 = 1$ kpc, and $q = 1$ (i.e. spherically symmetric assumption), while McMillan (2017) includes a single bulge with $\zeta = 2$, $\alpha = 1.8$, $r_0 = 0.075$ kpc, and $q = 0.5$ (i.e. an axially symmetric assumption). All best-fit parameter values in their models are given in Table 6. The volume mass density of the stellar disc component,

$$\rho_d(R, z) = \frac{\Sigma_{0,d}}{(2z_d)^{\eta}} \exp\left(-\frac{|z|}{z_d} - \frac{R}{R_d}\right). \quad (3)$$

Here, $\Sigma_{0,d}$ is the central surface density, z_d is the scale height, and R_d is the scale length. Sofue (2013) uses a flat stellar disc approximation (i.e. $z_d = 0$ and $\eta = 0$), while McMillan (2017) uses thin and thick stellar discs with $z_d = 0.3$ and 0.9 kpc, respectively, and $\eta = 1$. The surface density and the scale radius of the two models are given in Table 6. In addition to stellar discs, McMillan (2017) uses two gas discs representing H_1 and H_2 gas in the Galaxy. These gas discs are defined with mass densities

$$\rho_g(R, z) = \frac{\Sigma_{0,d}}{4z_d} \exp\left(-\frac{R_m}{R} - \frac{R}{R_d}\right) \text{sech}^2(z/2z_d), \quad (4)$$

with holes in their centres. The H_1 and H_2 discs have scale height z_d of 0.085 kpc and 0.045 kpc, and central hole scale

Table 6. The parameters of the main Galactic mass distribution model SOF13 used in this analysis, i.e. Sofue (2013) with updated values given in Sofue (2017). This model uses two bulges (i.e. inner and main), a stellar disc, and a dark halo. For comparison, we use MCM17 in the analysis and its relevant parameters are also given (McMillan 2017). This model uses only a single bulge with two stellar (i.e. thin and thick) and two gas discs (i.e. H_1 and H_2), and a dark halo. The central volume ($\rho_{0,b}$) and surface mass density ($\Sigma_{0,d}$) parameters are given in units of M_{\odot}/pc^3 and M_{\odot}/pc^2 , respectively, and the radii are given in kpc.

Model	Bulge $\rho_{0,b}, r_{\text{cut}}$	Disc $\Sigma_{0,d}, R_d$	Dark halo $\rho_{0,h}, h$
SOF13	Inner: 3.7×10^4 , 0.0035 Main: 2.1×10^2 , 0.12	292, 4.9	0.029, 10
MCM17	98.4, 2.1	Thin: 896, 2.5 Thick: 183, 3.02 H_1 : 53.1, 7 H_2 : 2180, 1.5	0.00854, 19.6

radius R_m of 4 kpc and 12 kpc, respectively. In both Sofue (2013) and McMillan (2017), the dark matter halo is defined as having mass density

$$\rho_h(R, z) = \frac{\rho_{0,h}}{X(1+X)^2}, \quad (5)$$

where $X = \sqrt{R^2 + z^2}/h$ and $\rho_{0,h}$ and h are the scale density and core radius, respectively. The fitting procedure and the best-fit values for the above parameters are given in Sofue (2017) and McMillan (2017), and also in Table 6 of this study.

Using the above components and the central BH, we estimate the total volume mass density of the Galaxy as a function of radius R (see the *top* panel in Fig. 3). Based on mass density, we then estimate the mass distribution (i.e. the total mass interior to a given radius R) of the Galaxy (see the *bottom* panel in Fig. 3). For further comparison, we also use previously published Galactic mass distribution models (Piffl et al. 2014; Binney & Tremaine 2008; Dehnen & Binney 1998) with their best fit parameters and calculate the volume mass density and the mass distribution as a function of radius (see Fig. 3). It can be seen that all these additional models were focused on the regions beyond the bulge and thus, derive similar variations in their density and mass curves to those derived from McMillan (2017) model. We note that the Galactic models in Dehnen & Binney (1998) are derived for the outer Galaxy and thus, its density and mass estimates are not meaningful at radii $R \lesssim 8$ kpc. As shown in Fig. 3, the model derived in Sofue (2013) provides more features and better constraints within the inner region of the Galaxy, particularly in the bulges where our pulsars are likely to be located.

We further note that some Galactic mass models suggest that there is a need for a ‘‘barred bulge’’ component in the central region of the Galaxy (e.g., McWilliam & Zoccali 2010; Nataf et al. 2010; Gardner & Flynn 2010; Ness et al. 2012). These models are non-axisymmetric and are typically computationally expensive to implement. By compar-

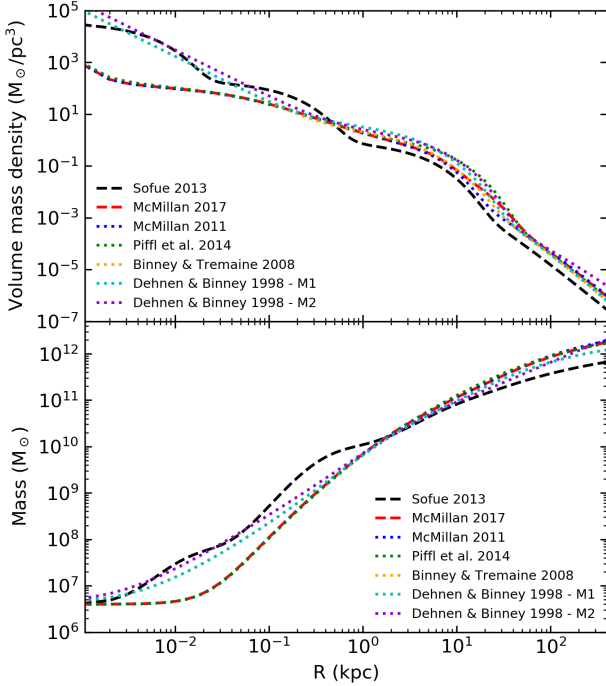


Figure 3. The volume mass density (*top*) and the mass distribution (*bottom* – i.e. the mass interior to radius R) of the Galaxy as a function of radius R measured from the GC. The different colours show the different Galactic models used. Note that the Sofue (2013) model with updated values given in Sofue (2017) provides better constraints within the inner Galaxy, in particular in the bulge regions. Other models mainly focus on the regions beyond the bulge and follow similar constraints. The Dehnen & Binney (1998) models were derived for the outer Galaxy and thus, they do not provide meaningful results when $R \lesssim 8$ kpc. Since the Galactic central BH is included in all models, their mass distributions converge to the BH mass of $4.2 \times 10^6 M_{\odot}$ when $R \rightarrow 0$. We use Sofue (2013) as our main model to constrain the properties of our pulsars.

ing the Sofue (2013) model and the bar/bulge model given in Portail et al. (2017), we noticed that the mass distribution at a given radius of the two models are consistent with each other. Compared to an axially symmetric model, a bar/bulge model can cause a slight difference in the Galactic gravitational potential along the LOS of the pulsar depending on the orientation of the bar component, leading to a slight change in our results. However, this change is within the uncertainties of our estimated \dot{P}_{int} values and pulsar distances. Therefore, we simply use the above mentioned axially symmetric Galactic mass models in this study.

We first calculate the gravitational potential Φ at the pulsar location (R, z) due to the Galactic mass distribution, and then estimate the Galactic acceleration in R and z directions, namely $-d\Phi/dR$ and $-d\Phi/dz$. To do this, we use the computer software GalPot¹⁰ (McMillan 2017, 2016), which computes the Galactic potential and the acceleration for any given Galactic mass distribution model. This software was based on Dehnen & Binney (1998) and the details of the computation are given in McMillan (2017). We note that

since all these Galactic mass models are axially symmetric (see Eq. 2 – 5), the acceleration does not depend on the azimuthal angle. Once the acceleration components of the pulsar and the Sun at their given locations in the Galaxy in R and z directions are computed, we can estimate the relative LOS acceleration a/c of the pulsar with respect to the Sun (see § 5.1). The acceleration a/c varies with the distance to the pulsar, providing a negative (or positive) value when the pulsar is located behind (or in front of) the sky-plane.

We estimate the maximum possible LOS acceleration curves a_{max}/c due to the Galactic potential as a function of Galactic longitude for a given Galactic latitude (see Fig. 4). We plot the absolute values of $|\dot{P}_{\text{obs}}/P|$ of PSRs J1748–3009, J1753–2819, J1757–2745, and J1804–2858 in the figure. Due to the axially symmetric mass distribution and the acceleration, we map the pulsars that are located in the fourth quadrant of the Galaxy in the first quadrant and include their \dot{P}_{obs}/P in the figure. It is evident that, as shown in Fig. 4, all our six PSRs J1746–2758, J1748–3009, J1753–2819, J1757–2745, J1801–3210, and J1804–2858 have much lower $|\dot{P}_{\text{obs}}/P|$ than the maximum Galactic accelerations along their LOSs obtained from our main Galactic model (Sofue 2013). Therefore, we cannot simply neglect the Galactic contribution in their observed \dot{P} . We investigate the LOS accelerations of these pulsars in detail in § 5.3, leading to limits on their intrinsic \dot{P} values. Fig. 4 also shows that most of the known pulsars that are located within the same field of view have much larger \dot{P}_{obs}/P compared to their Galactic maximum accelerations. If their Shklovskii terms are small, we can simply assume that the observed \dot{P} measurements of these pulsars are approximately equal to their intrinsic values. In addition, PSRs J1723–2837, J1727–2946, J1751–2857, and J1804–2717 have observed \dot{P}_{obs}/P that are comparable to the maximum Galactic accelerations along their LOSs (see *black* dots in Fig. 4). We note that the DM measurements of these pulsars are relatively small (between $19 - 60 \text{ cm}^{-3} \text{ pc}$; Hobbs et al. 2004b; Crawford et al. 2013; Lorimer et al. 2015; Desvignes et al. 2016) compared to those of our pulsars in the analysis (see Table 1). The DM-derived distances (using YMW16 model) to these pulsars are in the range of $0.72 - 1.9$ kpc (note that the NE2001 model derived distances are also in a similar range). This indicates that they are located close to the Sun and thus, the Galactic contributions in their observed \dot{P} values are insignificant, which means that the observed \dot{P} values are approximately equal to their intrinsic values.

5.3 Constraining the intrinsic period derivatives of pulsars

We know that \dot{P}_{int} and thus, \dot{P}_{int}/P , of a non-accreting pulsar is positive. As described before, a_{μ}/c is a positive contribution and thus, the measured negative \dot{P}_{obs} measurements of PSRs J1748–3009, J1753–2819, J1757–2745, and J1804–2858 can only be explained with a negative a/c Galactic contribution (see Eq. 1). Using a Galactic model as shown in § 5.2, we can compute the minimum possible Galactic acceleration (a_{min}/c) along a given LOS. Therefore, we can write the upper limit of the intrinsic period

¹⁰ <https://github.com/PaulMcMillan-Astro/GalPot>

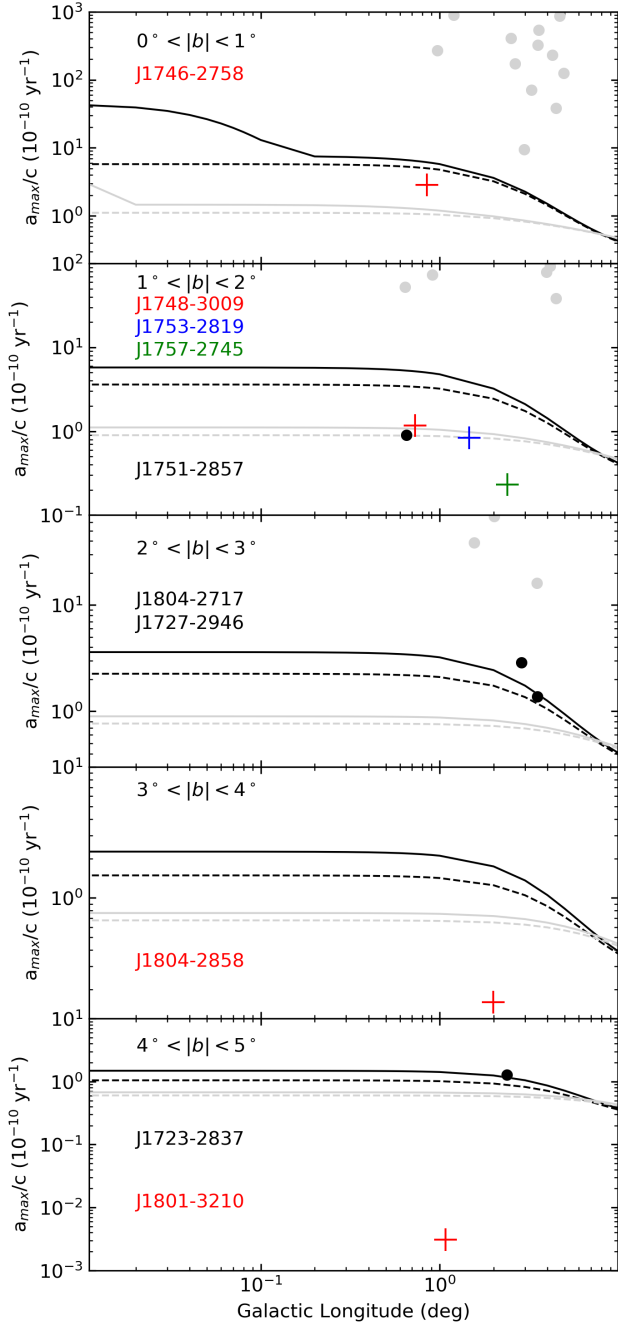


Figure 4. The estimated maximum LOS acceleration values (*black curves*) based on the main Galactic model (*Sofue 2013*) used in our analysis, as a function of Galactic longitude for various Galactic latitudes (see each panel). There are two separate acceleration curves shown in each panel corresponding to the lower (*solid*) and the upper (*dashed*) bound of the Galactic latitude used. The values of \dot{P}_{obs}/P of pulsars in our study are marked with crosses and the colour-code represents different sources as named in each panel. For clarity, we plot the absolute value of \dot{P}_{obs}/P of PSRs J1748–3009, J1753–2819, J1757–2745, and J1804–2858. For comparison, we also plot \dot{P}_{obs}/P of known pulsars (*grey dots*), and marked them with *black dots* and include their names in *black* if they are comparable (less than a factor of four) to the model-dependent maximum acceleration. Note that if the pulsar is located in the fourth quadrant of l , then we plotted $360^\circ - l$. For comparison, we also include the maximum LOS acceleration curves (*grey curves*) obtained from the Galactic model given in *McMillan (2017)*.

Table 7. The derived parameters of pulsars in the study. The minimum Galactic acceleration a_{min}/c is obtained from the Galactic model given in *Sofue (2013)*. The model-dependent upper limit on the intrinsic \dot{P} is derived using Eq. 6 (see § 5.3). The last column represents the model-dependent distance to the pulsar determined through dynamics as described in § 5.4. Note that for PSRs J1757–2745, J1801–3210, and J1804–2858, we quote the derived distances obtained using their timing measured proper motion limits.

PSR	a_{min}/c (10^{-10} yr^{-1})	\dot{P}_{int} (10^{-19} s/s)	D (kpc)
J1746–2758	−6.70	<148	<7.50 or >8.16
J1748–3009	−5.64	<1.38	8.24 – 8.99
J1753–2819	−4.36	<2.08	8.24 – 9.08
J1757–2745	−2.77	<1.42	8.27 – 9.40
J1801–3210	−1.48	<0.35	8.20 – 15.50
J1804–2858	−1.83	<0.08	8.32 – 9.40

derivative for these four pulsars to be

$$\left(\frac{\dot{P}_{\text{int}}}{P}\right)_{\text{upper}} = \frac{\dot{P}_{\text{obs}}}{P} - \frac{a_{\text{min}}}{c} - \frac{a_{\mu}}{c} \quad (6)$$

using Eq. 1. We first estimate the Galactic acceleration curves of these pulsars along their LOSs and plot in Fig. 5. We then estimate a_{μ}/c assuming the pulsar moves with a space velocity of either 100 km/s (*black dashed line*) or 320 km/s (*black dotted line*) and over-plot in the same figure. For clarity, the x-axis in Fig. 5 represents the distance L measured from the sky-plane (see Fig. 2 for definitions). Appendix A describes the calculation of a_{μ}/c in detail. We then estimate the model-dependent upper limit on the intrinsic \dot{P} of PSRs J1748–3009, J1753–2819, J1757–2745, and J1804–2858 using Eq. 6 with the Galactic accelerations shown in Fig. 5. The estimated limits are given in Table 7. PSRs J1757–2745 and J1804–2858 have measured values on their proper motions (see Table 4). For comparison, we estimate the Shklovskii contribution based on these measured proper motions in Right Ascension and over-plot in Fig. 5 (see the *orange curves*).

In addition to the observed \dot{P} , the timing solution of PSR J1748–3009 places a limit on its orbital period derivative \dot{P}_{b} (see Table 3). The timing parameters indicate that the pulsar is in a compact binary system with a period of 2.9-d and possibly in orbit with a white dwarf (the mass of the companion is $0.08 - 0.20 M_{\odot}$ with a median of $0.1 M_{\odot}$). Therefore, we can assume that the observed \dot{P}_{b} includes contributions from both dynamics and the emission of gravitational waves (see *Taylor & Weisberg 1989; Stairs et al. 2002; Kramer et al. 2006*). Thus, the observed \dot{P}_{b} provides important information to estimate the intrinsic period derivative of the pulsar independently. This approach has been used previously in several studies (e.g., *Matthews et al. 2016; Freire et al. 2017; Prager et al. 2017*). Similar to Eq. 1, we can express the pulsar LOS acceleration in terms of observed \dot{P}_{b} as follows:

$$\frac{\dot{P}_{\text{b}}}{P_{\text{b}}} = \left(\frac{\dot{P}_{\text{b}}}{P_{\text{b}}}\right)_{\text{GR}} + \frac{a}{c} + \frac{a_{\mu}}{c}, \quad (7)$$

where $(\dot{P}_{\text{b}}/P_{\text{b}})_{\text{GR}}$ is the expected contribution due to grav-

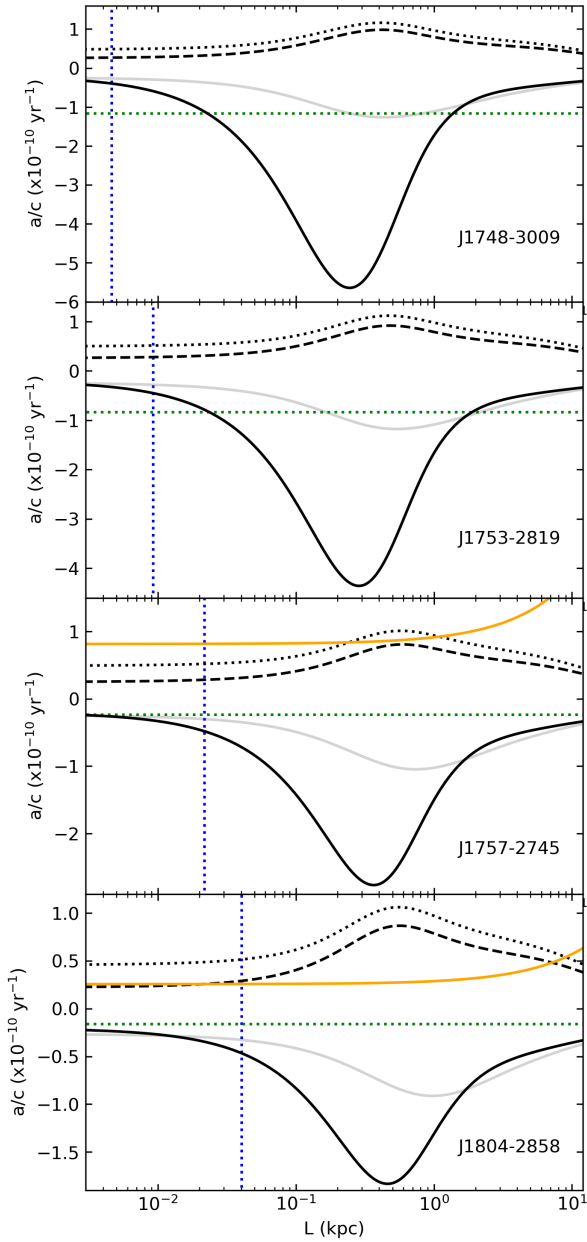


Figure 5. The Galactic LOS acceleration values of PSRs J1748–3009, J1753–2819, J1757–2745, and J1804–2858 as a function of distance L measured from the sky plane (see Fig. 2) along their LOSs based on Sofue (2013) (black solid) and McMillan (2017) (grey solid). The green dotted line represents the observed \dot{P}/P based on the timing measurements. The blue dotted line represents the distance measured from the sky plane of the pulsar to the plane which passes through the GC normal to the line joining the observer and the GC – i.e. $r_{\perp} \tan(\theta)$ (see Fig. 2). The black dashed and dotted lines represent the expected Shklovskii contribution for an assumed 100 km/s and 320 km/s space velocities, respectively. The estimated Shklovskii contribution based on the measured proper motion limits of PSRs J1757–2745 and J1804–2858 are over-plotted separately (orange line).

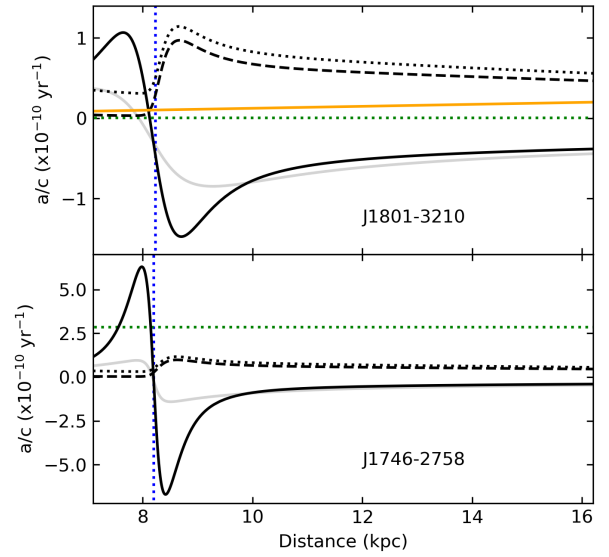


Figure 6. Same as Fig. 5, but for PSRs J1801–3210 and J1746–2752. Note that the x-axis is the distance measured from the Sun along the pulsar LOS.

itational wave emission. Assuming General Relativity, the expected $(\dot{P}_b)_{\text{GR}}$ is -4.3×10^{-16} s/s (using Eq. 8.52 in Lorimer & Kramer 2005, assuming a pulsar mass of $1.4 M_{\odot}$ and $\cos(i) = 0.5$, resulting in a companion mass of $0.1 M_{\odot}$), which is significantly smaller than the observed \dot{P}_b limit of $-2.6(10) \times 10^{-11}$ s/s. This indicates that the origin of the observed \dot{P}_b is most likely induced by the dynamical acceleration component of the pulsar along the LOS, similar to the observed \dot{P} measurement discussed earlier. Therefore, we can simply assume that $(a/c + a_{\mu}/c) \approx \dot{P}_b/P_b$ from Eq. 7 and then substitute that in to Eq. 1 to deduce \dot{P}_{int} independently, and it is calculated to be $(9.7 \pm 8.0) \times 10^{-19}$ s/s, where the uncertainty is 2σ . Note that this measurement is greater than the upper limit constrained above using the Galactic mass model (see Table 7). The reason for this discrepancy could be that we only have a limit on \dot{P}_b through timing, so that the above estimated \dot{P}_{int} from Eq. 7 is not well constrained.

As given in Table 4, the timing model of PSR J1801–3210 shows a positive, but extremely small \dot{P} . Given that PSR J1801–3210 is located towards the GC (with an angular separation of $4^{\circ}7'$ – see Table 5) and has a large DM, it is probable that the measured \dot{P} is dominated by the acceleration of the pulsar due to the Galactic potential. If $\dot{P}_{\text{obs}} < \dot{P}_{\text{int}}$, the contribution a/c must be negative (see Eq. 1). We plot the acceleration components given in Eq. 1 for this pulsar along its LOS in Fig. 6. Following the same method as above, we can then estimate the model-dependent upper limit on its intrinsic \dot{P} using Eq. 6, leading to a value of 3.5×10^{-20} s/s (see Table 5). This limit is broadly consistent with the measured \dot{P} values of unaccelerated millisecond pulsars with a similar period and we suspect that it is closer to the intrinsic \dot{P} value of the pulsar.

PSR J1746–2758 has a positive \dot{P} measurement of $4.42(5) \times 10^{-18}$ s/s, but this value is slightly smaller than that of the majority of other known pulsars that have a

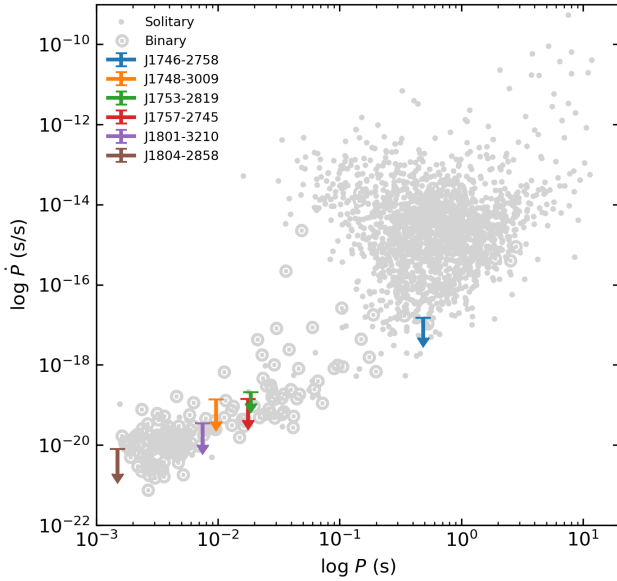


Figure 7. The P and \dot{P} diagram generated using all the known pulsars in the catalogue¹². The derived model-dependent intrinsic period derivative limits of the pulsars in this analysis as given in Table 7. We note that these limits are broadly consistent with the known pulsar population.

similar period (§ 4.6). Given that it is located towards the GC, with an angular separation of $0^\circ.96$, and also has a large DM, it is possible that the observed \dot{P} of PSR J1746–2752 is also influenced by its LOS acceleration. Therefore, we estimate the acceleration curves of this pulsar following the same procedure as described above (see Fig. 6). Using Eq. 6, we then estimate the upper limit on its intrinsic \dot{P} to be 1.48×10^{-17} s/s, which is approximately a factor of 3 larger than the measured value.

We finally plot the dynamically-derived model-dependent intrinsic \dot{P} limits of all our pulsars with their measured P values together with those of other known pulsars in Fig. 7. It is clear that the dynamically-derived \dot{P} limits of our pulsars are broadly consistent with those of other pulsars. Using these upper limits on \dot{P} values, we estimate and present the lower limits on characteristic ages and upper limits on surface magnetic fields in Table 3 and 4 (using Eq. 3.12 and 3.15 given in Lorimer & Kramer 2005).

5.4 Dynamical constraints on pulsar distances

Using the LOS acceleration values shown in Figures 5 and 6, we can simply estimate the intrinsic period derivatives \dot{P}_{int} of PSRs J1746–2758, J1748–3009, J1753–2819, J1757–2745, J1801–3210, and J1804–2858 as a function of distance using Eq. 1 (see Fig. 8 and 9). By definition we know that \dot{P}_{int} is positive and thus, these curves can be used to constrain the model-dependent distances to these pulsars. Using the known pulsar population, we can impose possible lower limits on their \dot{P}_{int} values. To do that, we select known pulsars within a 50 per cent window around the period of

a given pulsar in our sample, and then obtain the lowest observed \dot{P} in that population. This lowest \dot{P} is used as the minimum possible \dot{P}_{int} for that given pulsar and it is plotted in Fig. 8 and 9 with horizontal *dashed* lines. Assuming that \dot{P}_{int} should be greater than this minimum limit, we constrain the distances to be (8.24–8.99), (8.24–9.08), (8.22–9.65), (8.25–9.64), and (8.40–8.90) kpc for PSRs J1748–3009, J1753–2819, J1757–2745, J1801–3210, and J1804–2858, respectively (see Table 5). We notice that the lower limits of these distances are beyond the distances to the plane which passes through the GC perpendicular to the line joining the Sun and the GC along their LOSs, placing all these five pulsars on the far-side of the Galaxy. The distance to PSR J1746–2758 is not well constrained (see Fig. 9), although, it is likely to be located at a distance of either <7.5 kpc or >8.16 kpc. In all the above distance estimates, we assume Sofue (2013) as our main Galactic model and the peculiar velocity of the pulsar to be 100 km/s when calculating the Shklovskii contribution. If the velocity is larger than this assumed value, then \dot{P}_{int} decreases (i.e. the intrinsic curve shifts downward along y-axis) and thus, constrains the distance to a smaller range. Moreover, using the timing-measured proper motion limits of PSRs J1757–2745, J1801–3210, and J1804–2825, we estimate the Shklovskii contribution and then derive \dot{P}_{int} as before (see *orange* curves in Fig. 8 and 9), leading to more conservative pulsar distances of (8.27–9.40), (8.20–15.50), and (8.32–9.40) kpc, respectively.

Note that, as we mentioned in § 5.2, the McMillan (2017) model mainly focuses beyond the bulge regions and thus, it cannot be used accurately to constrain the distances to these pulsars. This can be seen in Fig. 8 and 9 as the model-derived \dot{P}_{int} values (*grey* solid curves) are potentially smaller than the minimum possible \dot{P}_{int} values (*dashed black* horizontal lines).

5.5 Comparison of dynamic-derived distances with DM-derived distances

The thermal free electron density model NE2001¹³ (Cordes & Lazio 2002) is widely used to estimate the distances to pulsars based on their measured DM obtained through timing. More recently, Yao et al. (2017) (YMW16¹⁴) re-evaluated the electron density model by using more recent independent pulsar distance observations. We compare our dynamically-estimated distances for PSRs J1748–3009, J1753–2819, J1757–2745, J1801–3210, and J1804–2825 given in § 5.4 with their DM-derived distances obtained from these electron density models. Note that we do not use PSR J1746–2758 in this comparison since its distance is not well constrained. We first use the YMW16 and NE2001 models separately to estimate the DM along the LOS of these pulsars (see Fig. 10). Note that we take account of a typical 20 per cent error on these DM values and indicate it with the shaded region in the figure. Based on the measured DM values, we find that the DM-derived distances obtained from the YMW16 model for PSRs J1748–3009, J1757–2745, J1801–3210, and J1804–2825 are consistent

¹² <http://www.atnf.csiro.au/research/pulsar/psrcat/>

¹³ <https://www.nrl.navy.mil/rsd/RORF/ne2001>

¹⁴ <http://119.78.162.254/dmodel/index.php>

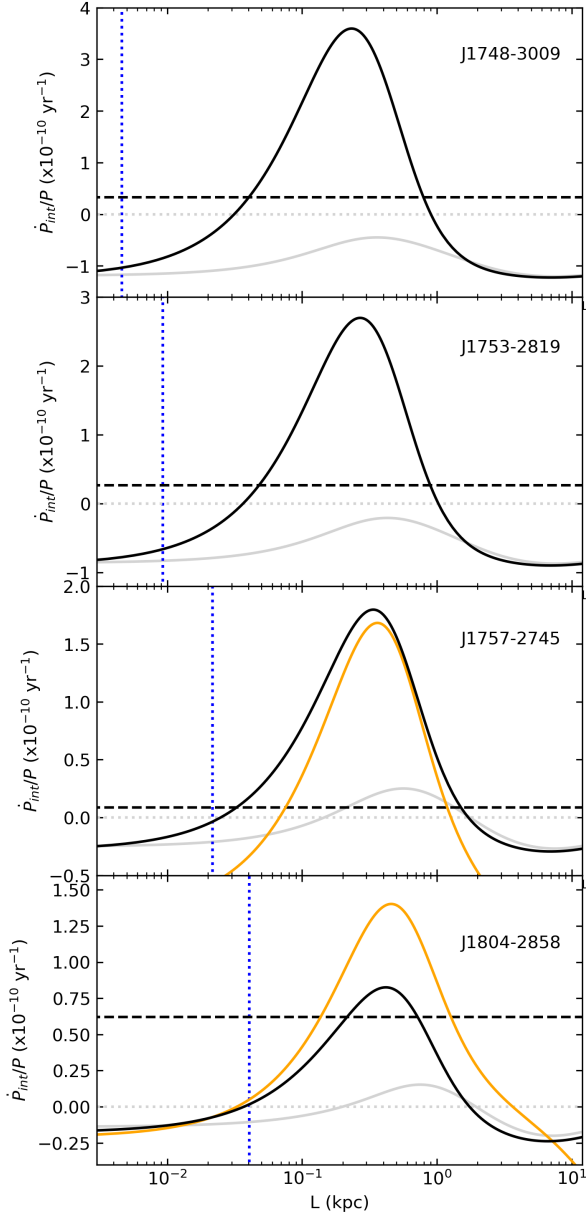


Figure 8. The model-estimated values of \dot{P}_{int}/P obtained using Eq. 1 based on dynamic acceleration and Shklovskii contributions given in Fig. 5 for PSRs J1748–3009, J1753–2819, J1757–2745, and J1804–2858 (black solid – Sofue (2013); grey solid – McMillan (2017)). Note that a pulsar space velocity of 100 km/s is assumed in the estimation of \dot{P}_{int}/P . The blue dotted line represents the distance measured from the sky plane to the plane which passes through the GC normal to the line joining the observer and the GC (see Fig. 2). The dashed black horizontal line represents the lowest measured \dot{P}/P value determined from the known population of pulsars around the spin period of the particular pulsar (see the text), and the distance range is estimated when \dot{P}_{int}/P is greater than this value. The estimated distances are given in Table 5 based on the Sofue (2013) model. Note that L represents the distance measured from the sky plane along the LOS. To get the pulsar distance, the distance to the sky plane from the Sun along the LOS (i.e. $R_{\odot} \cos(\theta)$, where $R_{\odot} = 8.2$ kpc and θ is the angular separation of the pulsar – see Table 5) should be added to L (see Fig. 2). The orange lines present the derived \dot{P}_{int}/P curve using the Shklovskii contribution estimated from the measured proper motion limits of PSRs J1757–2745 and J1804–2858.

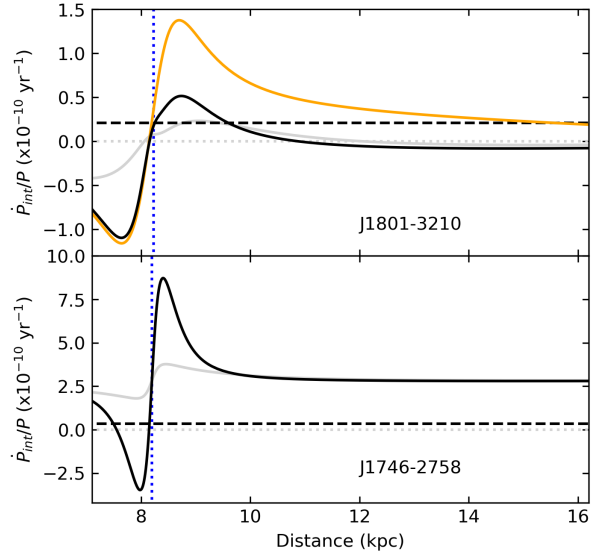


Figure 9. Same as Fig. 8, but for PSRs J1801–3210 and J1746–2758. Note that the x-axis represents the distance measured from the Sun along the pulsar LOS.

with our dynamics-derived distances within their uncertainties. For PSR J1753–2819, the DM-derived distance from YMW16 is small compared to its dynamics-derived distance. This indicates that the electron density predicted from YMW16 along the LOS of PSR J1753–2819 is overestimated, resulting in underestimated distance. As shown in the figure, the DM-derived distances obtained from NE2001 model for all of these pulsars are underestimated compared to their dynamics-estimated distances. By comparing the two models, it is seen that in general the distances estimated by the NE2001 model are underestimated (as reported before, see, e.g., Kramer et al. 2003) compared to those estimated by the YMW16 model at a given DM along the LOSs of these pulsars.

We consider all known pulsars that are located within an angular radius of 5° from the GC (i.e. $\theta < 5^\circ$) and plot their projected distances in the Galactic plane (see Fig. 11). Note that, we use DM-derived distances for these pulsars using the YMW16 model and assume a typical 20% uncertainty. We also plot our dynamically-derived distances for PSRs J1748–3009, J1753–2819, J1757–2745, J1801–3210, and J1804–2858 in the same figure. As can be seen, our distance estimates have much smaller uncertainties compared to the DM-derived distances, and these five pulsars are located on the far-side of the Galaxy.

6 DISCUSSION AND CONCLUSION

We report on the timing of recently discovered PSR J1753–2819, a 18.6 ms pulsar in a 9.3-hr binary orbit. We included this pulsar along with PSRs J1746–2758, J1748–3009, J1757–2745, J1801–3210, and J1804–2858 using LT and PKS observations to understand their \dot{P} measurements. The improved timing baselines indicate significant negative \dot{P} measurements for PSRs J1748–3009, J1753–2819, J1757–2745, and J1804–2858 (see Table 3

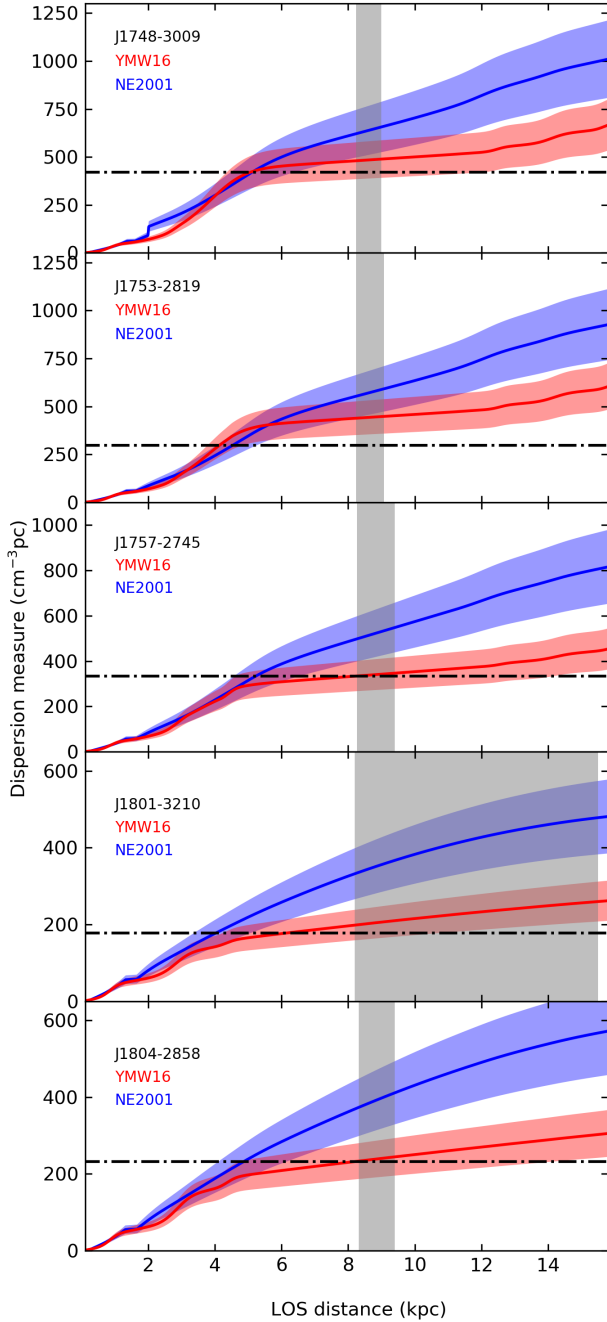


Figure 10. The DM values obtained from YMW16 (red) and NE2001 (blue) electron density models for our pulsars as a function of distance along their LOSs. The shaded blue and red regions represent the typical 20 per cent uncertainty of these models. The horizontal dot-dashed line represents the DM value of the pulsar (see Table 1). The grey shaded region represents the constrained model-dependent distances to these pulsars through our dynamic analysis (see § 5.4 and Table 7).

and 4). This is the first non-globular cluster pulsar sample that has observed negative \dot{P} measurements in their timing solutions, and they all lie within a few degrees of the GC. In addition, the timing of PSR J1801–3210 confirmed that it has an extremely low positive \dot{P} measurement, which provides the lowest measured value for a pulsar to date.

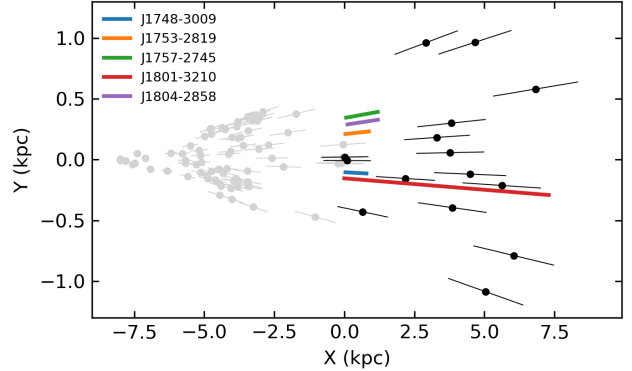


Figure 11. The observed pulsars located within an angular radius of 5° in the direction of the GC. A projection onto the Galactic plane is shown in cartesian coordinates. Note that the GC is at (0, 0) and the Sun is at (−8.2, 0.0) kpc. The distances are obtained from the YMW16 model for pulsars that are located on the near-side (grey dots) and the far-side (black dots), separately. The typical 20 per cent uncertainties of the distances are shown. The distances obtained from dynamics for PSRs J1748–3009, J1753–2819, J1757–2745, J1801–3210, and J1804–2858 in this study are over-plotted with different colours.

Since pulsars are powered by the loss of rotational kinetic energy, they spin-down gradually with a positive intrinsic \dot{P} . Therefore, the negative \dot{P} measurements of PSRs J1748–3009, J1753–2819, J1757–2745, J1804–2858 and the extremely small \dot{P} measurement of PSR J1801–3210 are not intrinsic, but induced by dynamics. We modelled the observed \dot{P} values of these pulsars as being due to dynamical acceleration in the Galactic potential along their LOSs. The analysis constrained the model-dependent upper limits on the intrinsic \dot{P} of these pulsars and they are broadly consistent with those of known pulsars (see Fig. 7 and Table 7). Using these model-dependent intrinsic \dot{P} values, we then constrained possible pulsar distances, indicating that PSRs J1748–3009, J1753–2819, J1757–2745, J1801–3210, and J1804–2858 are located on the far-side of the Galaxy (see Fig. 11 and Table 7). This is the first time that dynamics have been used to measure the distances to pulsars that are located in the far-side of the Galaxy.

The timing solutions of three pulsars in our sample measured limits on their proper motions (see Table 4). Assuming the Galactic model (Sofue 2013) is correct and $\dot{P}_{\text{int}} > 0$, we can determine the maximum possible total proper motion for PSRs J1757–2745, J1801–3210, and J1804–2858 and they are estimated to be 19.2, 12.6, and 13 mas/yr (using Eq. 1). These maximum possible total proper motions are consistent with our timing-measured limits given in Table 4. If the high-significance timing-measured proper motions in the future for these pulsars are greater than the above mentioned values, we can validate the Galactic model and also include any required additional features in the model to explain the observed pulsar motions.

As shown in Fig. 10, our dynamics-derived distances and the DM-derived distances from the YMW16 electron density model for these pulsars are consistent with each other in general within their uncertainties. However, the NE2001 model-derived distances are inconsistent with the

dynamics-derived distance. This could be due to difficulties in modelling the electron densities in the inner regions of the Galaxy with high stellar densities and large gas and dust contents towards the centre. Therefore, the independent distance measurements obtained to the pulsars in this study can be used to further improve electron density models.

PSRs J1748–3009, J1753–2819, and J1801–3210 are in binary systems and the timing results indicate that their companions are likely to be white dwarfs. Using the measured \dot{P}_b limit of PSR J1748–3009, we derived an independent limit on its intrinsic \dot{P} . Following a similar method, we will be able to measure \dot{P}_b values of these binary pulsars in the future with more observations and thus, derive their intrinsic \dot{P} values independently with better accuracy (see Smits et al. 2011). These estimates then can be used to improve their distance measurements.

Most of the Galactic models assume that the mass distribution in the Galaxy is either axially or spherically symmetric for simplicity, in particular within the bulge region. Having more pulsars in the Galactic centre region, we can use their observations to derive dynamics independently to study the Galactic potential, and then update and validate Galactic models including clumpiness in the mass distribution. We can also obtain independent distances to these GC pulsars in the future through parallax measurements using interferometers such as VLBI and then use them in deriving the Galactic potential. The next generation telescopes, such as the Square Kilometre Array, are useful with their outstanding capabilities to discover more pulsars in the GC region and to allow a comprehensive study to constrain the Galactic potential in the central region using pulsar timing in the future.

ACKNOWLEDGMENTS

Pulsar research at the Jodrell Bank Centre for Astrophysics and the observations using the Lovell Telescope are supported by a consolidated grant from the STFC in the UK. The Parkes radio telescope is part of the Australia Telescope, which is funded by the Commonwealth of Australia for operation as a National Facility managed by the Commonwealth Scientific and Industrial Research Organisation (CSIRO). D.R.L. acknowledges support from NSF RII Track I award number OIA–1458952 and is part of the NANOGrav Physics Frontiers Center which is supported by NSF award 1430284. R.S. acknowledges support from the Australian Research Council grant FL150100148. MB acknowledges ARC Grant CE170100004 (OzGrav).

REFERENCES

Abuter R., et al., 2019, arXiv e-prints,
 Bassa C. G., et al., 2016a, *MNRAS*, **456**, 2196
 Bassa C. G., et al., 2016b, *MNRAS*, **460**, 2207
 Bates S. D., et al., 2011, *MNRAS*, **416**, 2455
 Binney J., Tremaine S., 2008, *Galactic Dynamics: Second Edition*.
 Princeton University Press
 Bland-Hawthorn J., Gerhard O., 2016, *ARA&A*, **54**, 529
 Bland-Hawthorn J., et al., 2019, *MNRAS*,
 Blandford R., Teukolsky S. A., 1976, *ApJ*, **205**, 580

Brunthaler A., et al., 2011, *Astronomische Nachrichten*, **332**, 461
 Cordes J. M., Lazio T. J. W., 2002, preprint
 ([arXiv:astro-ph/0207156](https://arxiv.org/abs/astro-ph/0207156))
 Corongiu A., Possenti A., Lyne A. G., Manchester R. N., Camilo
 F., D’Amico N., Sarkissian J. M., 2006, *ApJ*, **653**, 1417
 Crawford F., et al., 2013, *ApJ*, **776**, 20
 Damour T., Taylor J. H., 1991, *ApJ*, **366**, 501
 Dehnen W., Binney J., 1998, *MNRAS*, **294**, 429
 Desvignes G., et al., 2016, *MNRAS*, **458**, 3341
 Eatough R. P., Keane E. F., Lyne A. G., 2009, *MNRAS*, **395**, 410
 Eatough R. P., Molkenthin N., Kramer M., Noutsos A., Keith
 M. J., Stappers B. W., Lyne A. G., 2010, *MNRAS*, **407**, 2443
 Eatough R. P., Kramer M., Lyne A. G., Keith M. J., 2013,
MNRAS, **431**, 292
 Edwards R. T., Hobbs G. B., Manchester R. N., 2006, *MNRAS*,
372, 1549
 Faulkner A. J., et al., 2004, *MNRAS*, **355**, 147
 Folkner W. M., Williams J. G., Boggs D. H., 2009, *Interplanetary
 Network Progress Report*, **178**, 1
 Folkner W. M., Williams J. G., Boggs D. H., Park R. S., Kuchynka
 P., 2014, *Interplanetary Network Progress Report*, **196**, 1
 Freire P. C., Camilo F., Kramer M., Lorimer D. R., Lyne A. G.,
 Manchester R. N., D’Amico N., 2003, *MNRAS*, **340**, 1359
 Freire P. C. C., et al., 2017, *MNRAS*, **471**, 857
 Gardner E., Flynn C., 2010, *MNRAS*, **405**, 545
 Genzel R., Pichon C., Eckart A., Gerhard O. E., Ott T., 2000,
MNRAS, **317**, 348
 Ghez A. M., Salim S., Hornstein S. D., Tanner A., Lu J. R., Morris
 M., Becklin E. E., Duchêne G., 2005, *ApJ*, **620**, 744
 Ghez A. M., et al., 2008, *ApJ*, **689**, 1044
 Gillessen S., Eisenhauer F., Trippe S., Alexander T., Genzel R.,
 Martins F., Ott T., 2009, *ApJ*, **692**, 1075
 Gonzalez M. E., et al., 2011, *ApJ*, **743**, 102
 Guinot B., 1988, *A&A*, **192**, 370
 Haslam C. G. T., Stoffel H., Salter C. J., Wilson W. E., 1982,
A&AS, **47**, 1
 Hobbs G., Edwards R., 2012, *Tempo2: Pulsar Timing Package*,
 Astrophysics Source Code Library (ascl:1210.015)
 Hobbs G., et al., 2004a, *MNRAS*, **352**, 1439
 Hobbs G., Lyne A. G., Kramer M., Martin C. E., Jordan C.,
 2004b, *MNRAS*, **353**, 1311
 Hobbs G., Lorimer D. R., Lyne A. G., Kramer M., 2005, *MNRAS*,
360, 974
 Hobbs G. B., Edwards R. T., Manchester R. N., 2006, *MNRAS*,
369, 655
 Hobbs G., et al., 2012, *MNRAS*, **427**, 2780
 Honma M., et al., 2012, *PASJ*, **64**, 136
 Hotan A. W., van Straten W., Manchester R. N., 2004, *PASA*,
21, 302
 Jacoby B. A., Cameron P. B., Jenet F. A., Anderson S. B., Murty
 R. N., Kulkarni S. R., 2006, *ApJ*, **644**, L113
 Kaspi V. M., Taylor J. H., Ryba M., 1994, *ApJ*, **428**, 713
 Keith M. J., Eatough R. P., Lyne A. G., Kramer M., Possenti A.,
 Camilo F., Manchester R. N., 2009, *MNRAS*, **395**, 837
 Knispel B., et al., 2013, *ApJ*, **774**, 93
 Kramer M., et al., 2003, *MNRAS*, **342**, 1299
 Kramer M., et al., 2006, *Science*, **314**, 97
 Lazaridis K., et al., 2009, *MNRAS*, **400**, 805
 Lorimer D. R., 2011, *SIGPROC: Pulsar Signal Processing Pro-
 grams*, Astrophysics Source Code Library (ascl:1107.016)
 Lorimer D. R., Kramer M., 2005, *Handbook of Pulsar Astronomy*.
 Cambridge University Press
 Lorimer D. R., et al., 2006, *MNRAS*, **372**, 777
 Lorimer D. R., et al., 2015, *MNRAS*, **450**, 2185
 Lynch R. S., Freire P. C. C., Ransom S. M., Jacoby B. A., 2012,
ApJ, **745**, 109
 Lyne A. G., et al., 1998, *MNRAS*, **295**, 743
 Manchester R. N., et al., 2001, *MNRAS*, **328**, 17

- Manchester R. N., Hobbs G. B., Teoh A., Hobbs M., 2005, *AJ*, **129**, i
- Matthews A. M., et al., 2016, *ApJ*, **818**, 92
- McMillan P. J., 2011, *MNRAS*, **414**, 2446
- McMillan P. J., 2016, GalPot: Galaxy potential code, Astrophysics Source Code Library (ascl:1611.006)
- McMillan P. J., 2017, *MNRAS*, **465**, 76
- McWilliam A., Zoccali M., 2010, *ApJ*, **724**, 1491
- Mickaliger M. B., 2013, PhD thesis, West Virginia University
- Mickaliger M. B., et al., 2012, *ApJ*, **759**, 127
- Mickaliger M. B., McEwen A. E., McLaughlin M. A., Lorimer D. R., 2018, *MNRAS*, **479**, 5413
- Morello V., et al., 2019, *MNRAS*, **483**, 3673
- Morris D. J., et al., 2002, *MNRAS*, **335**, 275
- Nataf D. M., Udalski A., Gould A., Fouqué P., Stanek K. Z., 2010, *ApJ*, **721**, L28
- Navarro J. F., Frenk C. S., White S. D. M., 1996, *ApJ*, **462**, 563
- Ness M., et al., 2012, *ApJ*, **756**, 22
- Ng C., et al., 2014, *MNRAS*, **439**, 1865
- Ng C., et al., 2015, *MNRAS*, **450**, 2922
- Nice D. J., Taylor J. H., 1995, *ApJ*, **441**, 429
- Perera B. B. P., et al., 2017, *MNRAS*, **468**, 2114
- Petit G., 2003, in 35th Annual Precise Time and Time Interval (PTTI) Meeting, San Diego, December 2003. pp 307–317
- Petit G., Tavella P., 1996, *A&A*, **308**, 290
- Piffl T., et al., 2014, *MNRAS*, **445**, 3133
- Portail M., Gerhard O., Wegg C., Ness M., 2017, *MNRAS*, **465**, 1621
- Prager B. J., Ransom S. M., Freire P. C. C., Hessels J. W. T., Stairs I. H., Arras P., Cadelano M., 2017, *ApJ*, **845**, 148
- Ransom S., 2011, PRESTO: Pulsar Exploration and Search Toolkit, Astrophysics Source Code Library (ascl:1107.017)
- Reid M. J., Menten K. M., Zheng X. W., Brunthaler A., Xu Y., 2009, *ApJ*, **705**, 1548
- Reid M. J., et al., 2014, *ApJ*, **783**, 130
- Schönrich R., 2012, *MNRAS*, **427**, 274
- Schönrich R., Binney J., Dehnen W., 2010, *MNRAS*, **403**, 1829
- Shklovskii I. S., 1970, *SvA*, **13**, 562
- Smits R., Tingay S. J., Wex N., Kramer M., Stappers B., 2011, *A&A*, **528**, A108
- Sofue Y., 2013, *PASJ*, **65**, 118
- Sofue Y., 2017, *PASJ*, **69**, R1
- Stairs I. H., Thorsett S. E., Taylor J. H., Wolszczan A., 2002, *ApJ*, **581**, 501
- Taylor J. H., 1992, *RSPTA*, **341**, 117
- Taylor J. H., Weisberg J. M., 1989, *ApJ*, **345**, 434
- Vasiliev E., 2019, *MNRAS*, **484**, 2832
- Verbunt F., Igoshev A., Cator E., 2017, *A&A*, **608**, A57
- Wolszczan A., Kulkarni S. R., Middleditch J., Backer D. C., Fruchter A. S., Dewey R. J., 1989, *New Astron.*, **337**, 531
- Yao J. M., Manchester R. N., Wang N., 2017, *ApJ*, **835**, 29
- van Straten W., Demorest P., Khoo J., Keith M., Hotan A., et al. 2011, PSRCHIVE: Development Library for the Analysis of Pulsar Astronomical Data, Astrophysics Source Code Library (ascl:1105.014)
- van Straten W., Demorest P., Osłowski S., 2012, *Astronomical Research and Technology*, **9**, 237

APPENDIX A: TRANSVERSE VELOCITY OF THE PULSAR AND THE SHKLOVSKII CONTRIBUTION

We denote the peculiar velocity of the Sun as $\vec{v}_{\odot,\text{pec}} = [U, V, W]$, where the unit vectors of the components are in the direction from the Sun towards the GC, in the direction of the Galactic rotation, and in the direction perpendicular

to the Galactic plane, respectively. Then the total velocity of the Sun

$$\vec{v}_{\odot} = [U, V + v_R(R_{\odot}), W], \quad (\text{A1})$$

where $v_R(R_{\odot})$ is the velocity of the local standard of rest for the Sun, or the circular Galactic rotational velocity at the radius of Sun R_{\odot} . For our calculation, we assume $[U, V, W] = [11.1, 12.24, 7.25]$ km/s (Schönrich et al. 2010) and obtain the Galactic rotation v_R from Galactic mass distribution models given in § 5.2. The main Galactic model we use in this study (Sofue 2017) results in $v_R(R_{\odot}) = 238$ km/s, which is the value they adopted in their model from Honma et al. (2012). Then the peculiar velocity, or the 3-dimensional space velocity, of the pulsar is defined as $\vec{v}_{\text{psr}} = [U_p, V_p, W_p]$ in the same coordinate system as before. The total velocity of the pulsar including its local standard of rest,

$$\vec{v}_{\text{psr}} = [U_p + v_R(R_p) \sin \theta', V_p + v_R(R_p) \cos \theta', W_p], \quad (\text{A2})$$

where $v_R(R_p)$ is the Galactic rotational velocity of the pulsar at its projected radial distance R_p on to the Galactic plane and θ' is the angle subtended at the GC between the position of the Sun and the projected position of the pulsar on the Galactic plane (see Fig. B.1 in Verbunt et al. 2017, for a schematic diagram). The angle θ' can be expressed as

$$\tan(\theta' + l) = \frac{R_{\odot} \sin l}{R_{\odot} \cos l - d \cos b}. \quad (\text{A3})$$

Using the above coordinate system, the relative velocity of the pulsar with respect to the Sun

$$\begin{aligned} \vec{v}_{\text{psr}} - \vec{v}_{\odot} &= [U_p + v_R(R_p) \sin \theta' - U, \\ &V_p + v_R(R_p) \cos \theta' - V - v_R(R_{\odot}), W_p - W]. \end{aligned} \quad (\text{A4})$$

To express the relative velocity in the Galactic coordinate system (l, b) , we write the unit vectors (\hat{l}, \hat{b}) in above coordinate system as

$$\begin{aligned} \hat{l} &= [-\sin l, \cos l, 0] \\ \hat{b} &= [-\cos l \sin b, -\sin l \sin b, \cos b]. \end{aligned} \quad (\text{A5})$$

We then write the relative velocity of the pulsar for its given (l, b) with respect to the Sun in Galactic coordinates as

$$\begin{aligned} v_l &= \hat{l} \cdot (\vec{v}_{\text{psr}} - \vec{v}_{\odot}) \\ &= -(U_p + v_R(R_p) \sin \theta' - U) \sin l \\ &\quad + (V_p + v_R(R_p) \cos \theta' - V - v_R(R_{\odot})) \cos l \end{aligned} \quad (\text{A6})$$

and

$$\begin{aligned} v_b &= \hat{b} \cdot (\vec{v}_{\text{psr}} - \vec{v}_{\odot}) \\ &= -(U_p + v_R(R_p) \sin \theta' - U) \cos l \sin b \\ &\quad - (V_p + v_R(R_p) \cos \theta' - V - v_R(R_{\odot})) \sin l \sin b \\ &\quad + (W_p - W) \cos b, \end{aligned} \quad (\text{A7})$$

respectively. We finally calculate the transverse velocity of the pulsar to be $v_T = \sqrt{v_l^2 + v_b^2}$. The derivation of the above expressions are given in Verbunt et al. (2017) in detail.

In § 5, for a given 3-dimensional pulsar space velocity of $|\vec{v}_{\text{p,pec}}|$, we randomly calculate $[U_p, V_p, W_p]$ (where $|\vec{v}_{\text{p,pec}}| = \sqrt{U_p^2 + V_p^2 + W_p^2}$), leading to a transverse velocity of v_T using Eq. A6 and A7. We perform 1000 trials for

a given $|\vec{v}_{\text{p,pec}}|$ and then obtain the average v_T , and then calculate the Shklovskii effect $a_\mu/c = v_T^2/cd$. We note that v_T is a function of R_p and thus, it varies along the LOS of the pulsar for a given $\vec{v}_{\text{p,pec}}$, and then a_μ/c . For instance, this variation in a_μ/c can be seen in Fig. 5.